Tailored Methodology based on Vapor Phase Polymerization to Manufacture PEDOT/CNT Scaffolds for Tissue Engineering

Antonio Dominguez-Alfaro,[a,b] *Nuria Alegret,*[a,b,c,*] *Blanca Arnaiz,*[a] *Jose M. González-Domínguez,*[d] *Ana Martin-Pacheco,*[d] *Unai Cossío,*[e] *Luca Porcarelli,*[b] *Susanna Bosi,*[f] *Ester Vázquez,*[d] *David Mecerreyes*[b,g,*] *and Maurizio Prato.*[a,f,g,*]

[a] Carbon Bionanotechnology Group, CIC biomaGUNE, Paseo de Miramón 182, 20014 Donostia-San Sebastián, Spain

[b] POLYMAT University of the Basque Country UPV/EHU, Avenida de Tolosa 72, 20018 Donostia-San Sebastián, Spain

[c] Cardiovascular Institute, UC Denver Anschutz Medical Campus, School of Medicine, 12700 E. 19th Avenue, Bldg. P15, Aurora, CO 80045, United States

[d] Departamento de Química Orgánica, Facultad de Ciencias y Tecnologías Químicas-IRICA, Universidad de Castilla-La Mancha, 13071 Ciudad Real, Spain

[e] Radioimaging and Image Analysis Platform, CIC biomaGUNE, Paseo de Miramón 182, 20014 Donostia-San Sebastián, Spain

[f] Department of Chemical and Pharmaceutical Sciences, INSTM. University of Trieste, Via L. Giorgieri 1, 34127 Trieste, Italy

[g] Ikerbasque, Basque Foundation for Science, 48013 Bilbao, Spain.

KEYWORDS: Carbon nanotubes, PEDOT, vapor phase polymerization, conductive polymers, 3D scaffold, tissue engineering, astrocytes

ABSTRACT. 3D Scaffolds with tailored stiffness, porosity and conductive properties are particularly important in tissue engineering for electroactive cell attachment, proliferation and vascularization. Carbon Nanotubes (CNTs) and poly(3,4-ethylenedioxythiophene) (PEDOT) have been extensively used separately as neural interfaces showing excellent results. Herein, we combine both materials and manufacture 3D structures composed exclusively of PEDOT and CNTs using a methodology based on Vapor Phase Polymerization (VPP) of EDOT onto a CNT/sugar composite. Such a strategy presents versatility to produce porous scaffolds, after leaching out the sugar grains, with different ratios of polymer/CNT, and controllable and tunable electrical and mechanical properties. The resulting 3D structures show Young's Modulus typical of soft materials (20-50 kPa), as well as high electrical conductivity, which may play an important role for electroactive cell growth. The conductive PEDOT/CNT porous scaffolds present high biocompatibility after 3 and 6 days of C8-D1A astrocytes incubation.

TOC Graphic

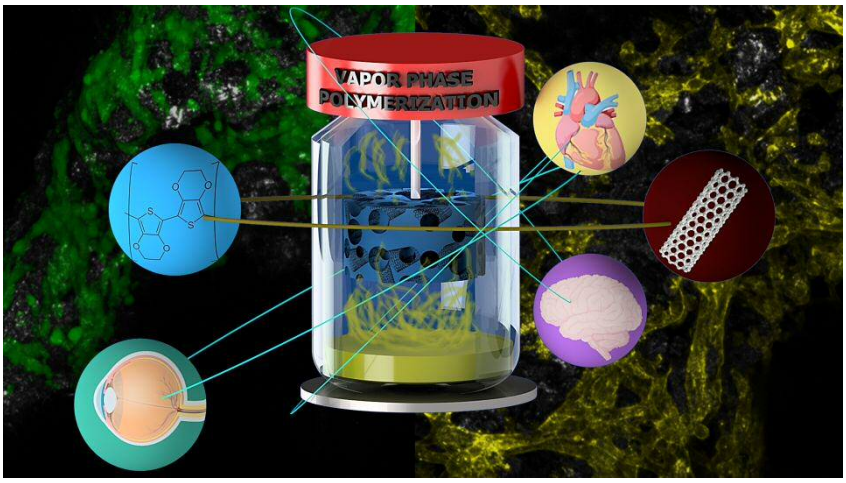
VAPOR PHASE
POLYMERIZATION

Introduction

Traumatic spinal cord injury afflicts approximately 180.000 people worldwide each year.[1–3] Within the first stages after the injury, neurons and glia in the trauma site lose function, which is then extended to the surrounded tissue. Consequently, necrotic cells around the cavity form a scar, inhibiting growth and generating a strong insulating barrier that blocks the communication between the nearby healthy cells.[4] Innovative solutions for such injuries require the development of materials able to feint this natural process. Such implantable materials must fulfill very specific characteristics, such as porosity to allow nutrient flow, conductivity to enhance the electroactive cellular growth, similar mechanical properties as the tissue of interest and biocompatibility to support cellular growth and attachment.[5]

Tissue engineering is focused on the development of the ideal implants to regenerate or replace the damaged tissue within a dysfunctional zone. Large number of publications have reported how cells grow and interact in planar dimensions,[5] although the human body represents a very complex three-dimensional cellular net, far from the bidimensional *in vitro* plate assays. Such a need to produce materials that simulate the complex matrix of the living systems set the 2D films aside to pave the way to 3D structures.[6] Tridimensional scaffolds stand out for their increase in structural complexity, surface area, effective

volume, and degree of porosity, thus providing gradients of nutrients and oxygen. Regarding electroactive cells, it has already been demonstrated that nerves, bones, muscle tissues, cardiac cells, and mesenchymal stem cells are sensitive to electrical materials and electrical stimuli,[7-10] thus pointing conductive polymers out (CP) as potential materials for their culture, recording and stimulation.[11,12] They possess electrical and optical properties similar to semiconductors, although their versatility, synthesis, biocompatibility and affordability are more attractive than common metals. Poly (3,4-ethylenedioxythiophene) (PEDOT) is the most used CP for a large number of applications, from energy storage or organic transistors to biomedical devices with living tisssues.[13–17] Commercial dispersions of PEDOT:PSS were already used to manufacture three dimensional foams for bioelectronic applications, showing ideal mechanical properties and conductivity for implants. The resulting devices were evaluated for organic electrochemical transistors, to analyze the culture of 3T3-L1s cell and to induce reorganization of proteins depending on PEDOT:PSS oxidized state.[18] As well, PEDOT:PSS platforms were tested for bone tissue engineering, demonstrating successful differentiation of osteogenic precursor cells (MC3T3-E1).[19] However, the presence of PSS produces delamination and decomposition of the manufactured films or coatings, making the replacement of the dopant a required need in biological

applications. Recently, Mantione *et al.* presented PEDOT dispersions based on the natural polymers GlycosAminoGlycan, which reduced the acidity of the residual sulfonate protons in PSS and improved the biocompatibility rate of long-term implants.[20] Recent studies used PEDOT:XanthamGum 3D scaffolds with tunable porosity and mechanical properties to monitor MDCK II eGFP cells growth.[21] On the other hand, only one recent study reported the use of Vapor Phase Polymerization (VPP) to produce PEDOT and polypyrrole (PPy) 3D structures *in situ*, using polystyrene microparticles as template for the final interconnected pores.[22]

Carbon Nanoforms are ideally suited for interaction with electroactive cells.[23] In particular, Carbon Nanotubes (CNTs) have attracted tremendous interest in the past decade due to their outstanding properties.[24] CNTs are distinguished by their excellent electrical and thermal conductivity, lightweight, mechanical properties and elasticity.[25] CNT films due to their nanotube morphology and electrical properties have been used for stimulation of neuron cells from the NG108 cell line, primary rat peripheral and hippocampal neurons.[26] Such studies showed that CNTs can boost the growth and function of neurons, evoking postsynaptic responses on hippocampal neurons, thus demonstrating potential for their electrical coupling.[27] Other electroactive tissues, as the heart, have shown similar results.[28–30] Polydimethylsiloxane (PDMS)/CNT scaffolds were manufactured to translate all

previous studies performed on 2D films to a more complex and closer to real 3D structures. Those foams resulted a genuine platform to grow and percolate neurons and neuroglia, linking the activity of living neurons networks.[31] Subsequently, Usmani *et al.* presented a very promising *in vitro* study where spinal cord explants were cultured on a sponge of CNTs producing spontaneous regrowth of the neurite within the tridimensional network, which supported the reconnection of the spinal cord segments.[10] Those porous 3D PDMS/CNT scaffolds biocompatibility was also assessed *in vivo*, showing high potential to exploit the use of 3D CNTs-hybrids in the area of regenerative medicine.[32]

The combination of carbon nanomaterials and conductive polymers represents a powerful tool to generate biohybrid materials able to promote tissue regeneration, to record information and stimulation.[33] We have previously developed a manufacturing method based on VPP, which allowed the modulation of the ratio PPy/CNT, their mechanical properties, porosity and conductivity.[34] In the present work, we use a similar methodology based on VPP to develop a hybridized material composed uniquely of PEDOT and CNT. Its different chemical and physical properties, such as low volatility, made it a challenge to manufacture tridimensional structures, thus the initial methodology has been modified to succeed. The resulting materials have been tested as biological platforms culturing C8-astrocytes,

obtaining spread cell over the cultured structure. C8-astrocyte morphology was also evaluated using microscopic techniques, which showed good cellular interconnectivity.

Experimental

Materials and Methods

Carbon Nanotubes (CNT, >95%) were purchased from Nanoamor Inc. (Stock# 1237YJS: inner diameter 5-10 nm; outside diameter 20-30 nm; length 0.5-2 μm). (3,4-ethylenedioxythiophene) (EDOT; 98%) and iron (III) p-toluene sulphonate hexahydrated ($Fe(Ts)_3$, technical grade) were purchased from Sigma-Aldrich. Iron (III) Chloride hexahydrated ($FeCl_3$) was ordered from Fisher. Ethanol (synthesis grade) was purchased from Carlo Erba Reagents SAS. All reagents and solvents were used as received with no further purification.

Thermogravimetric analyses were performed under air (25ml·min^{-1} flow rate) using a TGA Discovery (TA Instruments). The samples were equilibrated at 100°C for 20 min and then heated at a rate of 10°C·min^{-1}, in the range from 100°C to 800°C. X-ray Photoelectron Spectroscopy (XPS) measurements were performed using a SPECS SAGE HR 100 system spectrometer. A Mg Kα (1253.6 eV) X-ray source was employed operating at 12.5kV, at 8 and 10mA. The take-off angle was 90° and operating pressure was $8 \cdot 10^{-8}$ mbar. Quantitative

analysis of spectra was carried out using the Casa XPS 2.3 software.

Scanning Electron Microscope (SEM) measurements were performed on JEOL JSM-6490LV at 15kV, running in a point by point scanning mode. Micro-computed tomography (µCT) was used to quantify the porosity of the scaffolds. High resolution micro-CT scans were performed on a SkyScan 1172 µCT system (Bruker µCT, Kontich, Belgium) at an energy and intensity level corresponding to 33 kV voltage and 204 µA current for 1202 projections. Particle analysis toolbox in ImageJ was used to determine the pore size distribution of the scaffolds. Image processing protocol has been developed to assess scaffolds' surface porosity, pore size distribution and internal canalizations. Transmission Electron Microscope (TEM) was carried out on JEOL JEM-2100F model EM-20014, which features a 200 kV Field Emission Gun (Schottky) "FEG" and an Ultra High Resolution Pole Piece "UHR". Mechanical characterization was performed with a Mecmesin MultiTest 2.5-i dynamic mechanical analyzer, using a 50N load cell and Teflon-covered steel plates as holders. The conductivity was evaluated through the electrochemical impedance spectroscopy (EIS) using frequencies in the range from 0.1 to 1.000.000 Hz, with an electrochemical workstation Autolab MSTAT204 Potentiostat/Galvanostat.

Mouse astrocyte C8-D1A cell line was purchased from ATCC-LGC and cultured in phenol red-free DMEM media (GIBCO)

completed with 2 mM L-glutamine (Gibco), 100 $U \cdot ml^{-1}$ penicilline, 100 $\mu g \cdot mL^{-1}$ streptomycin (Gibco), 1mM sodium pyruvate and 10% heat-inactivated fetal bovine serum (Gibco). The PBS buffer was purchased in tablets and prepared following manufacturer procedures (Sigma-Aldrich), corresponding to 10 mM phosphate buffer containing 137 mM NaCl and 2.7 mM KCl at pH 7.4.

3D scaffolds synthesis and characterization

The 3D scaffolds were produced through a multi-stage process similar to the previously reported in our group.[31,34] 250 mg of crystal sucrose were mashed and sifted through two sieves with mesh sizes of 100 µm and 250 µm, respectively (Fisher Scientific Inc.). Crystal sugar grains in the middle fraction were collected, ensuring a grain size under 250 µm and above 100 µm. CNTs (15 mg) and the sieved sucrose (500 mg) were mixed and shaken overnight. Then, 7% of oxidant (Fe(Ts) or $FeCl_3$) were incorporated and blended until obtaining a homogeneous powder. Finally, 5 µL of MilliQ water were added and mixed. The resulting black blend was introduced inside a hollow plastic cylinder (Ø=5 mm) and compacted from both sides to form a cylindrical-shape template, which was then hanged with a thread inside a Schlenk flask. Subsequently, 0.4 mL of EDOT monomer were introduced at the bottom of the flask and the VPP was carried out under vacuum, varying two conditions: temperature (120°C

and 140°C), and time of reaction (6h and overnight). Once the polymerization was completed, the cylinder was immersed overnight into MilliQ water to dissolve the sucrose and the excess of oxidant, resulting in a self-standing architecture with interconnected micro-channels and holes. The scaffold was cleaned with ethanol for five days in a Soxhlet system until complete removal of iron byproducts and free PEDOT oligomers. Dynamic decay of iron and chlorine in the system after Soxhlet cleaning was evaluated using XPS.

Compressive modulus testing

Prior to mechanical testing, the scaffolds were soaked in Milli-Q water for 1-2 min, and the excess of water was carefully removed with a piece of Kimwipes®. Uniaxial compressive tests were performed under ambient conditions to the wet scaffold since it represents a more similar biological environment, at a rate of 15 $mm \cdot min^{-1}$, until reaching a 90% compressive strain. The extent of the deformation was measured by relating the measured height displacement at each point of the analysis with the scaffolds' initial height (strain, in %). The obtained force curve was normalized to the specimens' initial diameter (stress, in kPa). Young's Modulus was then obtained as the slope of the stress/strain curve of the linear elastic section in the initial stages (typically from 15 to 40% strain in our case). At least 4-5 repetitions of each sample were measured.

Scanning electron microscope (SEM)

The morphology on the scaffold's surface was analyzed by SEM. The samples were sliced in 2 mm thickness and evaluated in different magnifications. The sample was mounted on an aluminum holder with double-sided carbon tape.

Micro-computed Tomography (µCT)

Scaffolds were isolated from the background, using a thresholding procedure that was specific to this material. The values to segment the scaffold from background were optimized comparing the 2D grey scale image of a single slice with the threshold image. In this way, binary images were created and porosity values for each slice were assessed (see example in Figure S1). Porosity values were determined as the percentage of pores' area with respect to the total area. Since both scaffolds had some imperfections (big pores, d>500 µm) these regions or slices were discarded for the analysis. The analyzed areas in both samples are shown in Figure S1: the selected region for the first sample was between the slices 300 (Rec0300) and 655 (Rec0655) and between the slices 285 (Rec0285) and 650 (Rec0650) for the second. The material was highly homogeneous within the selected region for analyses, thus the porosity was calculated in 14 randomly selected slices (n=14) for the first sample, and 16 randomly selected slices (n=16) for the second.

µCT images were binarized using an optimized threshold and subjected to processing steps such as dilation, erosion and watersheding. To analyze the pore distribution, the area of each pore was measured, and the equation of a circle was used to estimate an approximate value of the diameter of the pore, according to equation 1:

$$Pores = 2x(\sqrt{\frac{A_{circle}}{\pi}}) \qquad (1)$$

Due to the high homogeneity of the system, the pore size distribution was calculated in n=10 2D-images randomly selected along the 3D object.

Transmission electron microscopy (TEM)

Intimate relationship between PEDOT and CNT was evaluated using TEM studies. Samples were prepared by adding a single drop (0.5 µL) of the aqueous solution (ca. 0.1 mg·mL^{-1} in milliQ water) of PEDOT/CNT powder, obtained by grinding the scaffolds, onto a copper grid coated with a carbon film (Electron Microscopy Sciences). The grid was left to dry under air for several hours at room temperature.

Conductivity measurements

Relative conductivity between PDMS/CNT and PEDOT/CNT scaffolds was evaluated using Impedance Electrochemical Spectroscopy (EIS). To carry out the measurement, a homemade device was developed (Figure S2). The scaffolds were cut into cylinders of 5 x 5 mm (LxD), immersed in phosphate-buffered saline (PBS, 10 mM) and degassed for 5 minutes to

ensure the complete permeation of the inner porous structure. Then, scaffolds were placed inside a PDMS container with few drops of 10 mM of PBS buffer solution. Two coplanar gold electrodes were placed in a sandwich conformation to complete the full structure and ensure the constant contact and electric flow within the 3D scaffold along the experiment.

Biocompatibility assay

Before the in vitro assays, the scaffolds were dipped in MilliQ water several times in order to ensure the removal of ethanol from the cleaning step. Then, they were left to dry in air and cut into thin disks of 2mm thickness. PDMS/CNT disks were cleaned under low-pressure oxygen plasma for 6 min (Pico Plasma Cleaner, Diener electronic) each side. Then, all the scaffolds were UV-sterilized on each side for 20 min.

Cell culture and counting. C8-D1A cells were cultured in complete media at 37 °C and 5% CO_2 in tissue culture-treated 75 cm^2-flasks (Nunc). For cell passage, cells were detached from the flasks by incubation at 37 °C with trypsin-EDTA solution 1X (2.5 g porcine trypsin and 0.2 g EDTA·4Na per liter of Hanks' Balanced Salt, Sigma) and spun at 103 RCF for 5 min; the obtained pellet was resuspended in 1 ml of complete media and disaggregated. For cell counting, the cell suspension was diluted 1:10 in PBS and 1:2 in the exclusion dye Trypan Blue solution (0.4% in 0.81% sodium chloride and 0.06% potassium phosphate, dibasic, Sigma). 10

µL of the diluted cell suspension was counted in a haemocytometer chamber under transmitted light in an inverted microscope (DMIL, Leica).

All the 3D scaffolds were placed in a 96-well sterile plate (Costar) and incubated in 200 µL complete media for 1h at 37 °C and 5% CO_2. For cell seeding, the media was removed by aspiration and 20-50 µl complete media containing $5 \cdot 10^5$ C8-D1A cells were seeded onto the scaffolds. The wells were filled by slowly adding 150 µL complete media and incubated for 3 and 6 days at 37 °C and 5% CO_2.

LDH assay. The viability of cells grown on the scaffolds was evaluated with the modified LDH CytoTOX96 Non-Radioactive Cytotoxicity Assay kit (Promega) reported by Ali-Boucetta *et al.*[35] For cell lysis, scaffolds were transferred to a 96-well U bottom plate and mechanically disrupted by smashing after addition of 150 µL of PBS containing 9%Triton X-100 (lysis buffer, LB). Then, the samples were frozen at -80°C for 30 min, defrosted for 20 min at 37 °C and disrupted again. The CNT-PEDOT-based material was separated by centrifugation at 1000 G for 10 min at 4 °C and supernatants were transferred to empty wells. For the LDH detection, 50 µL of each supernatant was mixed with 50 µL substrate mix and, after 4 min, the reaction was terminated by the addition of 50 µL of stop solution. Absorbance measurements at 492 nm were taken in a micro plate spectrophotometer (GeniosPro, Tecan). Positive control

diluted in LB 1:5000 was included as an internal control (not shown), and LB alone was used as negative control (not shown). All the collected data is represented as means of quadruplicates ±SD. Student's *t* test was performed to draw statistical comparisons between two treatment groups. Differences were considered statistically significant at $p < 0.05$.

Fluorescence staining of viable cells for microscopy. Calcein-AM (Molecular Probes) staining was performed to fluorescently label living cells. The scaffolds with cells were transferred to empty wells and incubated at 37 °C for 30 min with 200 µL of complete media containing 2.5 $\mu g \cdot ml^{-1}$ of Calcein-AM (Molecular Probes).

F-actin stain for cell morphology imaging. The scaffolds incubated with cells were transferred to empty wells, washed once with 200 µL PBS, fixed with 4% paraformaldehyde in PBS for 20 min at 20 °C, and washed twice with PBS. Then, the cells in the scaffolds were permeabilized with 0.2% Triton X-100 in PBS for 20 min at 37 °C. For cell F-actin filament staining, the scaffolds were incubated at 37 °C for 30 min in 200 µL of ActinGreen488 (1:10, Molecular Probes) in 0.1% Twee-20 PBS and washed twice with PBS before imaging.

Confocal imaging. Scaffolds with ActinGreen or Calcein-AM stained cells were placed in a 50 mm-diammeter ≠1.5 optical glass-bottom-petri dish (Mattek) and a drop of PBS alone or media containing 2.5 $\mu g \cdot ml^{-1}$ Calcein-AM was added,

respectively. Images were taken in a laser scanning microscope (lsm880 AxioObserver, Zeiss) employing excitation at 633 nm and detection between 615-670 nm in the reflection mode for scaffold imaging, and excitation at 488 nm with detection between 500-615 nm for Calcein-AM stained cells or ActinGreen488 stained cells. For live imaging, a microscope insert chamber was employed at 37 °C, 5% CO_2 and 100% humidity. Each image stack consisted of 55 dual-channel optical sections that were acquired at optimal intervals *of 2 µm* to reach a 100 µm-optical Z section with the Plan-Apochromat 20x/0.8 M27 objective. ZEN software was employed to generate a maximum intensity projection view from each Z-stack image. Single dual-channel images of 1µm optical section at higher magnifications using the Plan-Apochromat 63x/1.40 Oil DIC M27 objective were also collected.

SEM imaging of the cell morphology inside the scaffolds

After cell culture, dehydration of the samples with an ethanol in deionized water gradient (60%, 70%, 80%, 90%, and 100%) was carried out, each for 1 h at room temperature. Finally, a second dehydration was performed with a hexamethyldisilazane (HMDS) in ethanol gradient solutions (30%, 50%, 70%, 90%, 100%) using 30 minutes incubation for each step. After 1 hour in HMDS 100% samples were air-dried, sputter-coated with gold (Alto 1000, Gatan Inc.), and visualized by SEM operated in secondary electron detection mode.

Results and discussion

Manufacture and composition of PEDOT/CNT porous scaffolds by VPP

Vapor phase polymerization (VPP) is commonly employed to deposit thin film layers of conductive polymers such as PEDOT or PPy onto non-conductive substrates to provide electrical conductivity. In a pioneering work, Winter-Jensen and co-workers determined that iron-based catalysts, in particular iron (III) tosylate, yields the highest conductive bidimensional PEDOT films.[36] Aferwards, many studies demonstrated that other reaction conditions, such as additives, temperature, time and amount of oxidant, have also a crucial effect on the final conductivity, which can exceed 1000 $S \cdot cm^{-1}$.[37] In particular, a change in the temperature produces remarkable changes in the morphology of PEDOT, leading to an effect on the intercalation of the polymer chains and, thus, changes in the conductivity.[38,39] We hypothesized that such conditions have a similar effect and behavior for the coating of PEDOT in a 3D structure. Therefore, our first goal was to analyze and optimize the reaction conditions not only to obtain highly conductive devices, but also to produce self-standing tridimensional PEDOT/CNTs scaffolds.

Figure 1 describes the general synthetic procedure to manufacture VPP scaffolds. Briefly, a sucrose-CNTs-oxidant

template was hanged inside a sealed tube containing EDOT monomer. As usual in VPP methods, the temperature was increased, and the polymerization took place inside the template where the EDOT vapor reacts with the oxidant. In the final step, the porous PEDOT/CNT template was produced by immersing the material in water and dissolving the sugar grains and the oxidant impurities. The porosity was estimated using a given weight of sucrose with specific granulometry between 100-250 µm as porogen. The conditions for the EDOT gas reaction with the oxidant were established in terms of time (6 h and overnight) and temperature (120 °C and 140 °C). It is worth noting that lower temperatures and shorter times lead to collapse of scaffolds upon removal of sucrose, suggesting that not enough polymer was produced to hold the entire structure. Since EDOT presents a low volatility capacity (vapor pressure of 0.278 mmHg at 24°C), the VPP was performed under vacuum. The kind and amount of oxidant $Fe(Ts)_3$ or $FeCl_3$ (adding 20 mg, 40 mg or 80 mg) was also evaluated. However, only the scaffolds polymerized using 20 mg of $FeCl_3$ were stable keeping the 3D structure after the cleaning step. This fact can be explained due to the more powerful oxidant ability of $FeCl_3$ when compared to $Fe(Ts)_3$; furthermore, $FeCl_3$ has shown excellent results in the previously synthesized PPy/CNTs 3D scaffolds.[34] On the other side, we postulate that larger quantities of oxidant hinder the polymerization due to the high humidity from the hydrated

oxidant. As in previous works, Fabretto *et al.* pointed out that additional water absorption in PEDOT polymerization produces an increase in the formation of crystallite regions within the oxidant layer, which are not able to participate in an effective polymerization of EDOT.[40,41] The complete removal of Fe and Cl was confirmed by the lack of the corresponding signals in the XPS analyses (see Figure S3).

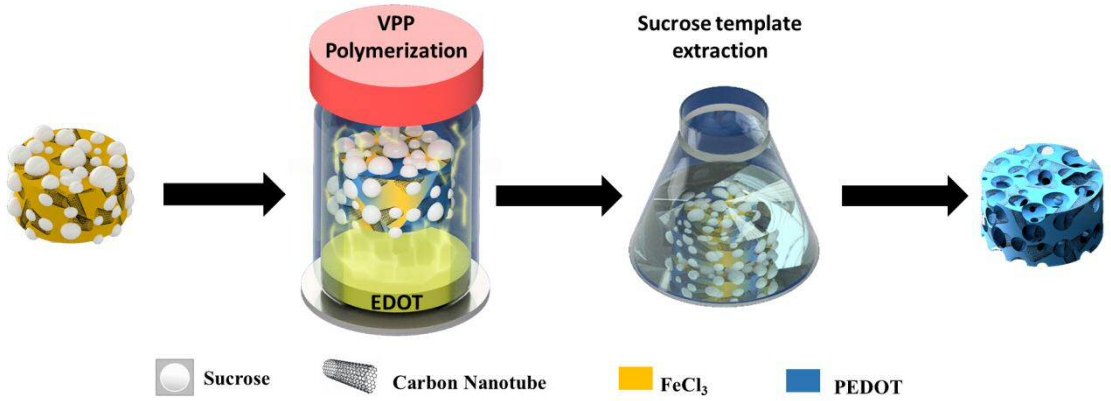

Figure 1. General scheme to manufacture PEDOT/CNT scaffolds: template formed using sugar grains as porogen or sacrificial template, CNTs and the oxidant; polymerization of PEDOT through VPP; and washing with water and ethanol to remove the sugar, reagents and side products.

TGA was used to evaluate the ratio of PEDOT and CNT for each preparation conditions. The resulting plots show two well-separated degradation curves (Figure 2a and first derivative curves in Figure S4): a first one between 100-500 °C, corresponding to the polymer loss, and a second starting around 500 °C that corresponds to the CNT degradation. The

amount of PEDOT polymerized was estimated in terms of percentage of weight loss per gram of sample at 500 °C, right before the degradation of CNTs begins, as shown in Figure 2a. The scaffolds' composition was determined between 42 and 68 wt% of PEDOT. According to the results collected in Table S1, there is an increase in the amount of PEDOT polymerized with time and/or temperature. The major effect was observed with a change in the temperature: an increase of 20 °C gives rise to *ca.* 25% more PEDOT deposition, while an increase in time from 6 h to overnight, results only in a 6% increase of PEDOT synthesized. These facts suggest that almost all the polymerization occurs within the first six hours of reaction. Additionally, we also corroborate that the PEDOT polymerization was homogeneous along the whole scaffolds by the analysis of several sections of the structure (see TGA plot in Figure S5).

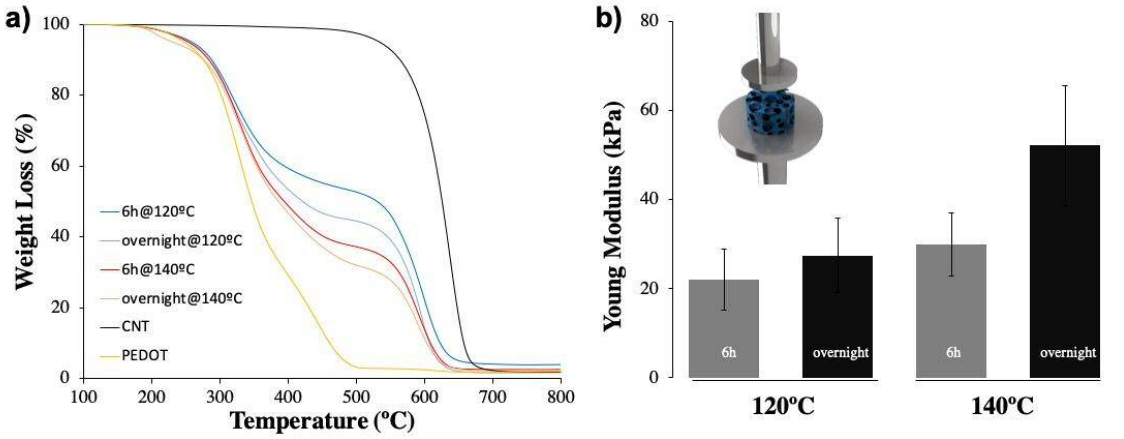

Figure 2. a) TGA plot under air and **b)** Young's Modulus (wet) of the scaffolds synthesized in different conditions

(*n*=5). Increase in time and temperature of synthesis yields to higher amount of PEDOT deposited and higher YM.

Mechanical properties of the PEDOT/CNT scaffolds

Compression tests of the wet scaffolds were performed to evaluate the Young's Modulus (YM's) of the manufactured scaffolds. No swelling behavior was observed. The results, reported in Figure 2b, show that the stiffness of the material increases with the time and temperature of polymerization, which are intimately correlated with the amount of polymer deposited within the scaffold (see Table S1 and Figure 2a). Interestingly, short periods of time, *i. e.* 6 h of reaction, and/or lower temperatures, *i. e.* 120 °C, results in similar YM's in the range of 20-30 kPa. Meanwhile, high temperatures and large times of polymerization (140 °C overnight) yields to more rigid scaffolds with the highest YM's values, *ca.* 50kPa. Such values are close to the ones reported for the spinal cord, thus suggesting good potential for these scaffolds in spinal cord tissue engineering.[42,43]

Morphology of 3D CNT/PEDOT porous Scaffolds

Cells cultured on 3D structures exhibit behaviors more similar to *in vivo* conditions than cells cultured on 2D substrates. This is the reason why in 3D structures porosity is a very important parameter to mimic the real environment of biological tissues. In general, an increase in the number

and size of pores, or the interconnectivity, usually leads to improved ECM secretion, cell infiltration, tissue ingrowth, and molecular delivery.[5]

Electron microscopy techniques were used to study the number and size of pores upon removal of sucrose, used as porogen or sacrificial template. The produced macropores inside the polymeric scaffold, of irregular shapes mimicking living tissue's irregular geometries, have been analyzed by SEM. Images in Figure 3 reveal a homogeneous porous and wrinkled morphology, plenty of interconnected holes and folds. In particular, two kinds of surface can be differentiated in the morphology of a hole: one smooth, which may be related to PEDOT, and one coarse with a brush-like shape placed in the frame of the cavities, which might correspond to disorganized assemblies of CNTs, as confirmed upon observing at higher magnifications. No differences were observed between the scaffolds synthesized by different conditions, as shown in Figure S6. Moreover, the morphology of the template before the sucrose dissolution was also analyzed and the planar surface with absence of holes observed (see Figure S7) confirmed that PEDOT has completely filled the empty spaces within the sucrose template.

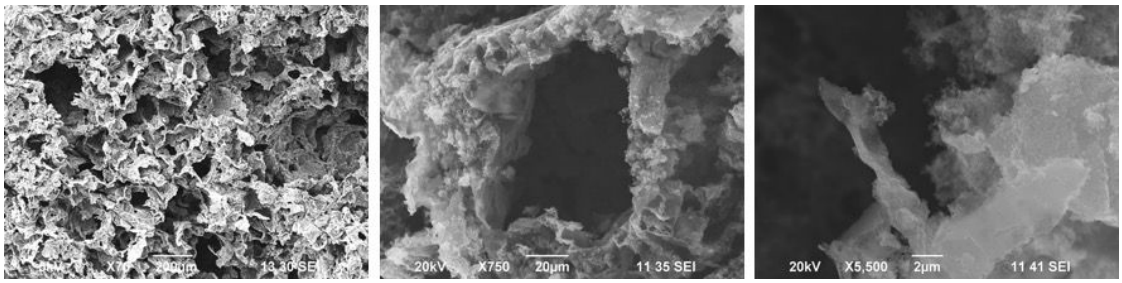

Figure 3. SEM micrographs of the 3D scaffolds (synthesized overnight at 140°C) that show the homogeneous micro-porosity. CNT are distributed over the polymeric surface, as distinguished in high magnification images.

Furthermore, micro-computed tomography (µCT) was used to quantify the micro-porosity of two PEDOT/CNT scaffolds and analyze its internal 3D structure (Figure 4). The analyzed areas in both samples are shown in Figure S1. The surface porosity value of these nanocomposite scaffolds was found to be 45.01 ± 2.86% (n=14 slices) in the first sample and 47.54 ± 4.09% (n=16 slices) in the second one. This means that close to 45% of the sample's area corresponds to pores and 55% to matter. Note the small standard deviation among slices, which reflects the homogeneity of the object and supports the random selection of a finite number of 2D slices for image analysis. In addition, the analysis of µCT images determined a structure formed mostly of macropores, composed of sizes between 20-300 µm. Two samples with different manufacture method conditions have been analyzed, and no significant differences between both pore size distributions were appreciated. As seen in Figure 4d, around 25% of the total pores are meso/micro pores, composing of pore size

below 50 µm, almost 60% between 50 and 100 µm, around 20% between 100 and 150 µm and less than 7% above 150 µm (see Figure S8 for a higher size resolution histogram).

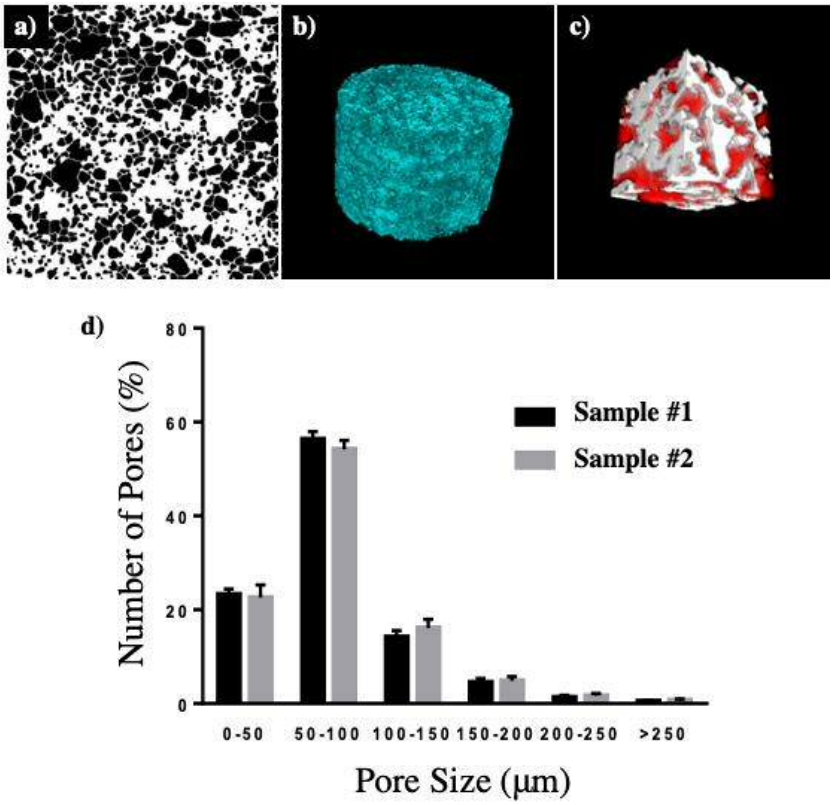

Figure 4. a) Transversal µCT binarized image (2D), where pores are represented in black color and matter (scaffold) in white. **b)** Whole scaffold's 3D volume rendered image. **c)** 3D illustration of scaffold's pore distribution; pores are represented in red color and matter in white. **d)** Pore size distribution of two PEDOT/CNT scaffolds' synthesized at different conditions (sample #1: 140°C overnight, *n=14*; sample #2: 120°C overnight, *n=16*). Note that there are no significant differences between samples.

TEM was employed to study the disposition and interaction between the polymer and the CNTs in the tridimensional nanostructure. PEDOT can polymerize in several nanometric forms, like nanorods, nanowires or nanoparticles, among others, depending on the polymerization conditions.[44-46] In our case, as shown in Figure 5, we can distinguish between three sub-structures: (i) thin tubes with diameters around 15-20 nm, corresponding to naked CNTs; (ii) thick tubes, which are assumed to be PEDOT/CNT hybrids with the polymer wrapping the cylindrical structures; and (iii) polymer film agglomerates, determined as PEDOT. TEM revealed that most of the CNT present in the scaffold are coated with the polymer, increasing the diameter up to 60 nm. It is worth noting that such heterogeneity may be responsible for the scaffold's structural integrity as the local agglomerates of polymer and polymer-wrapped CNT would underpin the whole structure. We hypothesize that the polymerization around CNT is mainly achieved through the non-covalent π-π stacking of the aromatic polymer backbone and the surface of the nanotubes. Such electrostatic interaction between conductive polymers through non-covalent functionalization has already been observed.[47-49] In principle, there could be covalent attachment of PEDOT to the CNTs. As a matter of fact, extensive functionalization of CNTs leads to loss of the electronic properties. Since we retain high values of

conductivity, we tend to believe that we have little or no reaction between PEDOT and MWNTs.REF Tour, J. Chem Eur J, 2004, 10, 812-817

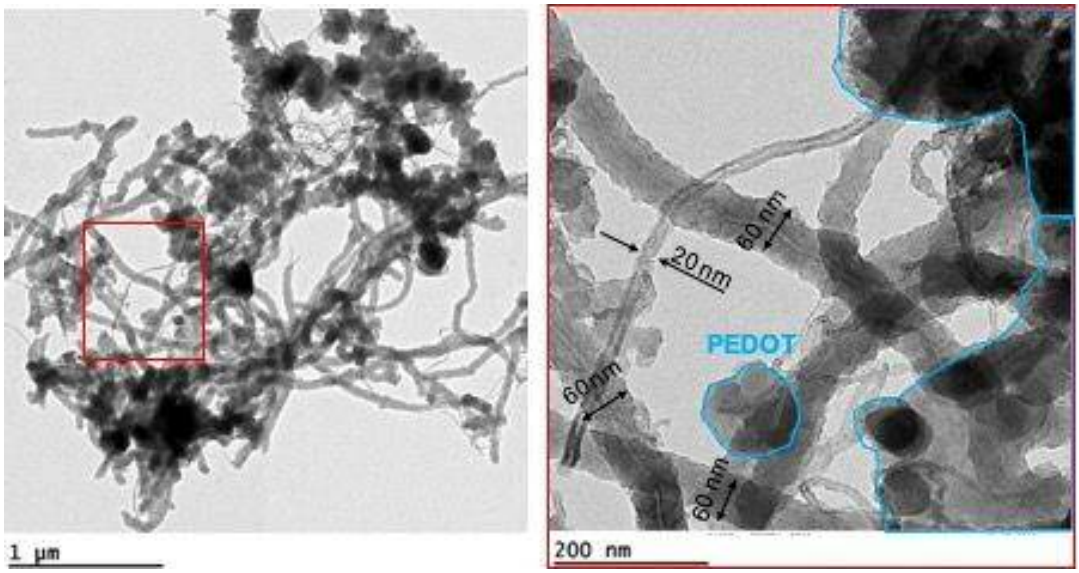

Figure 5. Interaction analyses of the nanotubes and the polymer *via* TEM micrographs of the CNT/PEDOT materials obtained. Note that some nanotubes increase in diameter due to the coating of the polymer, while in other regions small films of PEDOT helps in the cohesion of the whole structure and keep the tridimensionality.

Electrical properties of 3D PEDOT/CNT scaffolds

Electrochemical Impedance Spectroscopy (EIS) is a very powerful tool to evaluate the three-dimensional conductivity of the entire scaffold without destroying the sample. In contrast to classical electrochemical techniques that measure the charges or electrode potentials as a function of time, EIS generates a signal as a function of the frequency

at a constant potential. In addition, EIS provides a large number of variables (frequency, voltage, phase, current, etc.), thus a large amount of information that can be used, for example, to monitor the cell growth and colonization.[47] Such technique has already been used to evaluate the 3D conductivity in scaffolds composed of PEDOT used to support cellular activity.[51–54] Meanwhile, the conductive behavior of porous carbon electrodes used in materials chemistry for water deionization or as supercapacitors, has been analyzed through Bode and Nyquist plots.[55]

Figure 6 shows the Bode plot of the 3D scaffolds analyzed. The scaffolds were cut to obtain cylinders (Ø = 5 mm) of 5 mm height and placed inside the electrochemical cell compartment (see Methods) in contact with the two gold electrodes. The electrochemical impedance spectra were obtained in the frequency range between 0.1 Hz and 1000 kHz. As a reference, previously reported scaffolds composed of an insulating polymer, PDMS/CNT, with equal dimensions were also analyzed to evaluate the electrical contribution of CNTs. Our results show that the impedance of PEDOT/CNT ($|Z_{PEDOT/CNT}|$=6 kΩ) scaffolds at 0.1 Hz was approximately ten times lower than that of PDMS/CNT ($|Z_{PDMS/CNT}|$=50 kΩ), and one order of magnitude lower than the naked electrode filled with electrolyte PBS solution ($|Z_{PBS}|$=90 kΩ, see Figure S9). We hypothesize that the impedance behaviour of the PEDOT/CNT scaffolds might arise not only from the presence of the CNT

or the PEDOT themselves, but also from the conductive bridges formed between the conjugated thiophene chains of the PEDOT matrix and the CNT during the polymerization process.

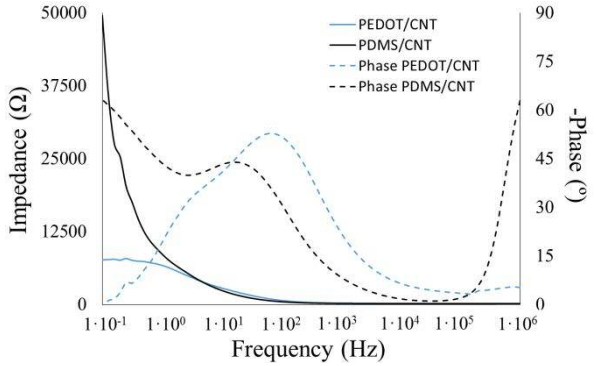

Figure 6. Conductivity measurement through impedance (solid line) and phase angle (dashed line) analyses *vs* frequency measurement of the scaffolds PEDOT/CNT (blue) and PDMS/CNT (black).

The Bode plot in Figure 6, shows that PEDOT/CNT scaffold present two responses in the phase: a maximum near medium frequencies, *ca.* 100 kHz, corresponding to a phase of 52°, and a small shoulder at lower frequencies. At the same time, PDMS/CNT present a band close to 10kHz, although the maximum phase is placed at 62°. The PEDOT/CNT scaffolds' phase Bode plot can be associated to a Randle circuit behavior due to the electrons flow through the entire matrix.

Additionally, according to the Nyquist plot (see Figure S10), the phase movement shows a capacitance behaviour at high frequencies and a resistor contribution (Phase = 0°) at lower frequencies. In contrast, the PDMS/CNT scaffolds show

capacitor behavior at low frequencies. Furthermore, the porous morphology of the scaffolds allows for a significantly higher surface-to-volume ratio, resulting in low impedance that is promising for neural probe applications.

In vitro biocompatibility of 3D PEDOT/CNT scaffolds

Mouse astrocytes C8-D1A were cultured on scaffolds for 3 and 6 days and *in vitro* cytotoxicity was analyzed using a modified Lactate Dehydrogenase (LDH) assay. This method has been reported previously to circumvent all interactions between CNT and the insoluble formazan crystals formed in the commonly used 3-(4,5-Dimethylthiazol-2-yl)-2,5-Diphenyltetrazolium Bromide (MTT) or conventional LDH viability tests, and thus assessing the impact of CNT-based material on cellular survival in a straightforward and reliable manner.[35] The LDH activity signal of the cytosolic fraction was taken as a semiquantitative measurement of the number of surviving cells in the scaffolds. Once the cells are lysed, the level of absorbance of the LDH product correlates with the number of viable cells growing on the scaffolds. As all the scaffolds were seeded with the same number of astrocytes, differences would be attributed to the effect of the materials on cell survival. The previously reported PDMS/CNT was analyzed for comparison.

In a first experiment, the effect of the different polymerization conditions employed was evaluated, *i.e.*

different PEDOT/CNT ratios, and showed no significant differences between the different kind of scaffolds (see Figure S11). In a second step, the PEDOT/CNT scaffolds were compared with the previously synthesized PDMS/CNT scaffolds, and, again, no significant differences in the absorbances were observed (see Figure 7a). These facts demonstrate not only the non-cytotoxicity of the different scaffolds developed, but also that the scaffolds manufactured have a positive impact on the C8-D1A growth yet in the first three days of culture.

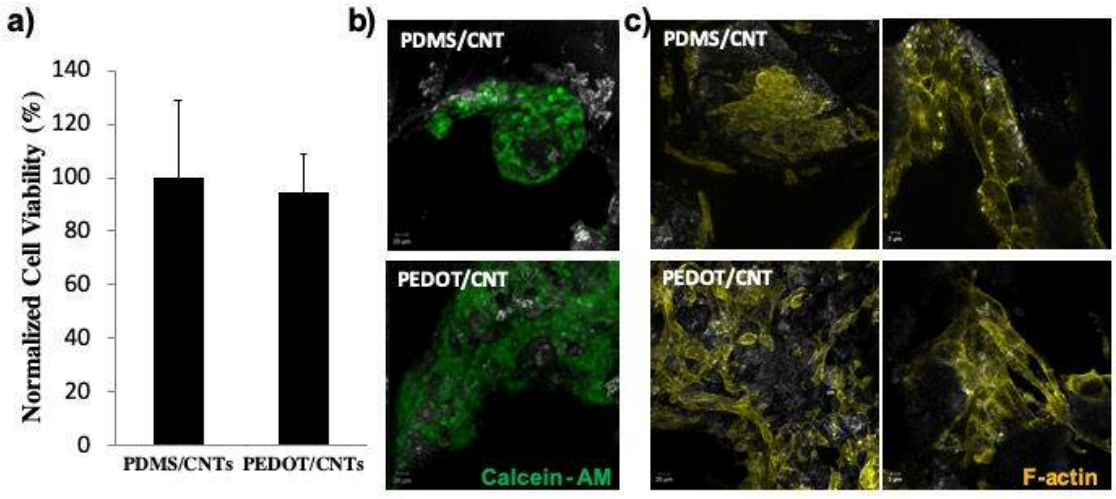

Figure 7. a) *In vitro* LDH assay of C8-D1A astrocytes cultivated for 3 days on scaffolds in the presence of 30% CNTs. Maximum projection view of Z-stack images after **b)** calcein-AM stain of viable cells (green) and **c)** the cell membrane F-actin (yellow) staining of PEDOT/CNT scaffolds after 3 days of culture. Merge view: stained cells (green or yellow), scaffold (grey). Images are fluorescent and

reflection acquisitions for C8-D1A and scaffolds by confocal microscopy, respectively. **a)** All values are expressed as means ± SD from 4 independent experiments (*n=3*). P>0.05, results are considered statistically non-significant by Student's *t* test.

In addition, confocal imaging was employed to analyze the cellular attachment to the PEDOT/CNT scaffold. Only living cells were stained with calcein-AM in fluorescent green after incubation in the scaffolds for 3 and 6 days. Furthermore, z-stacks showed certain degree of cell penetration within the range of visualization allowed by the objective working distance (up to 100 µm) through the pores of the scaffold (see Figures S12 and S13). The images in Figure 7b and Figures S12-S14 show high confluence of alive cells adhered to the scaffold, even after 6 days *in vitro*. The adhesion and proliferation of C8-D1A cells on PDMS/CNT scaffolds was also evaluated with calcein-AM staining for comparison, showing different growth behavior: astrocytes on PDMS/CNT scaffolds tend to grow forming clusters of cells, as shown in Figure 7b and Figures S12-S14, instead of spreading over the whole surface, as with the PEDOT/CNT scaffolds. Cluster formation produce a less homogenous biological active surface onto the material, decreasing their own growth stretching and the long-distance communication between them, having an effect on their natural activity presumably.[56]

Furthermore, the morphology of the astrocytes was analyzed by staining their cytoskeleton with filamentous actin (F-actin, Figure 7c). Large elongations of the filamentous axons of the cells was observed, indicating the typical phenotype of astrocytic cells. This is a clear indicator that the cells keep their original function.

SEM images of the cultured cells in Figure 8 confirmed that astrocytes maintain their normal morphology. Large elongations, as well as abundant cell-to-cell contacts (highlighted with green arrows), can be distinguished, suggesting the guidance and enhancement of the material during their growth and expansion, as previously reported.[33] This observation not only confirms the low cytotoxicity of the material, but also let us anticipate that the cells are also able to maintain their function.

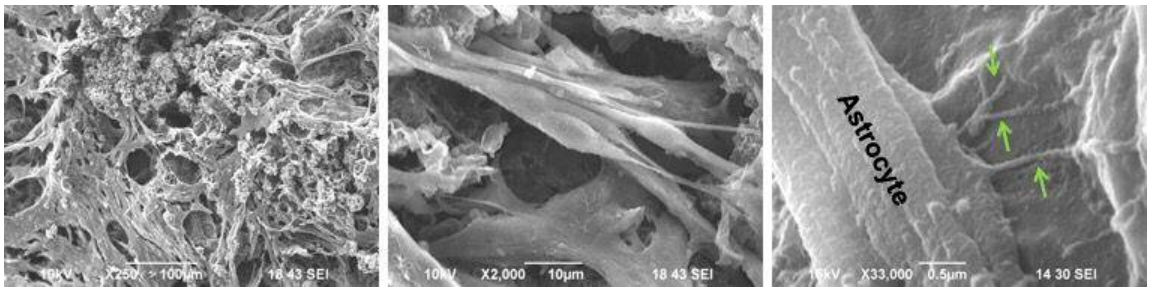

Figure 8. SEM images of the astrocytes grown in the 3D PEDOT/CNT scaffolds for 3 days. Higher magnifications show the close interaction and adhesion of the astrocytic filaments to the scaffold.

Conclusions

In this work, we have taken advantage of the VPP methodology to manufacture 3D porous scaffolds composed uniquely of PEDOT and CNT by using a sucrose template as sacrificial a porogen. This procedure represents a powerful tool to manufacture tridimensional scaffolds with controllable properties, including the polymer composition, porosity, conductivity and compressive toughness. The scaffolds' composition was modulated from 42% to 68% of PEDOT through different reactions conditions, as determined by TGA. Compressive experiments revealed YM's in the range of 20-50 kPa, typical values of soft systems. The resulting porosity, pore diameters and homogeneity obtained after the sucrose removal were analyzed using SEM and µCT, confirming high homogeneity, pore size mostly in the order of 50-100µm and excellent interconnectivity between them. As well, EIS analyses showed that the PEDOT/CNT scaffolds are highly conductive and have impedances ten times below the previously reported PDMS/CNT. Finally, high viability was demonstrated with the incubation of astrocytes. Overall, our results illustrate how the prepared scaffolds are suitable candidates for implants in neural tissue.

ASSOCIATED CONTENT

Supporting Information included.

AUTHOR INFORMATION

Corresponding Author

* NA. E-mail: nuria.alegret@ehu.es

* DM. E-mail: david.mecerreyes@ehu.es

* MP. E-mail: prato@units.it

Present Addresses

‡ Group of Carbon Nanostructures and Nanotechnology, Instituto de Carboquímica ICB-CSIC. C/ Miguel Luesma Castán 4, 50018 Zaragoza (Spain).

Author Contributions

The manuscript was written through contributions of all authors. All authors have given approval to the final version of the manuscript.

Funding Sources

The Spanish Ministry of Economy and Competitiveness MINECO (project CTQ2016-76721-R), the University of Trieste, Diputación Foral de Gipuzkoa program Red (101/16), the European Commission (H2020-MSCA-RISE-2016, grant agreement No 734381, acronym CARBO-IMmap) and ELKARTEK bmG2017 (Ref: Elkartek KK-2017/00008, BOPV resolution: 8 Feb 2018) are gratefully acknowledged for financial support. MP, as the recipient of the AXA Chair, is grateful to the AXA Research Fund for financial support. This work was performed under the Maria de Maeztu Units of Excellence Program from the Spanish State Research Agency – Grant No. MDM-2017-0720. NA

has received funding from the European Union's Horizon 2020 research and innovation programme under the Marie Sklodowska-Curie grant agreement No 753293, acronym NanoBEAT.

ABBREVIATIONS

VPP, Vapor Phase Polymerization; CNTs, Carbon; PEDOT, poly(3,4 ethylenedioxythiophene); CP, Conductive Polymers

REFERENCES

(1) Lee, B. B.; Cripps, R. A.; Fitzharris, M.; Wing, P. C. The Global Map for Traumatic Spinal Cord Injury Epidemiology: Update 2011, Global Incidence Rate. *Spinal Cord* **2013**, *52*, 110.

(2) Sekhon, L. H. S.; Fehlings, M. G. Epidemiology, Demographics, and Pathophysiology of Acute Spinal Cord Injury. *Spine (Phila. Pa. 1976).* **2001**, *26* (24S).

(3) Singh, A.; Tetreault, L.; Kalsi-Ryan, S.; Nouri, A.; Fehlings, M. G. Global Prevalence and Incidence of Traumatic Spinal Cord Injury. *Clin. Epidemiol.* **2014**, *6*, 309–331. https://doi.org/10.2147/CLEP.S68889.

(4) Martirosyan, N. L.; Carotenuto, A.; Patel, A. A.; Kalani, M. Y. S.; Yagmurlu, K.; Lemole, G. M.; Preul, M. C.; Theodore, N. The Role of MicroRNA Markers in the Diagnosis, Treatment, and Outcome Prediction of Spinal Cord Injury. *Front. Surg.* **2016**, *3*, 56. https://doi.org/10.3389/fsurg.2016.00056.

(5) Huang, G.; Li, F.; Zhao, X.; Ma, Y.; Li, Y.; Lin, M.; Jin, G.; Lu, T. J.; Genin, G. M.; Xu, F. Functional and Biomimetic Materials for Engineering of the Three-Dimensional Cell Microenvironment. *Chem. Rev.* **2017**, *117* (20), 12764–12850. https://doi.org/10.1021/acs.chemrev.7b00094.

(6) Alegret, N.; Dominguez-Alfaro, A.; Mecerreyes, D. 3D Scaffolds Based on Conductive Polymers for Biomedical Applications. *Biomacromolecules* **2019**, *20* (1), 73–89. https://doi.org/10.1021/acs.biomac.8b01382.

(7) Ghasemi-Mobarakeh, L.; Prabhakaran, M. P.; Morshed, M.; Nasr-Esfahani, M. H.; Baharvand, H.; Kiani, S.; Al-Deyab, S. S.; Ramakrishna, S. Application of Conductive Polymers, Scaffolds and Electrical Stimulation for Nerve Tissue Engineering. *J. Tissue Eng. Regen. Med.* **2011**, *5* (4), e17–e35. https://doi.org/10.1002/term.383.

(8) Jeong, S. I.; Jun, I. D.; Choi, M. J.; Nho, Y. C.; Lee, Y. M.; Shin, H. Development of Electroactive and Elastic Nanofibers That Contain Polyaniline and Poly(L-Lactide-Co-ε-Caprolactone) for the Control of Cell Adhesion. *Macromol. Biosci.* **2008**, *8* (7), 627–637. https://doi.org/10.1002/mabi.200800005.

(9) Shi, G.; Zhang, Z.; Rouabhia, M. The Regulation of Cell Functions Electrically Using Biodegradable Polypyrrole-Polylactide Conductors. *Biomaterials* **2008**, *29* (28), 3792—3798.

https://doi.org/10.1016/j.biomaterials.2008.06.010.

(10) Usmani, S.; Aurand, E. R.; Medelin, M.; Fabbro, A.; Scaini, D.; Laishram, J.; Rosselli, F. B.; Ansuini, A.; Zoccolan, D.; Scarselli, M.; et al. 3D Meshes of Carbon Nanotubes Guide Functional Reconnection of Segregated Spinal Explants. *Sci. Adv.* **2016**, *2* (7). https://doi.org/10.1126/sciadv.1600087.

(11) Guo, B.; Glavas, L.; Albertsson, A.-C. Biodegradable and Electrically Conducting Polymers for Biomedical Applications. *Prog. Polym. Sci.* **2013**, *38* (9), 1263–1286. https://doi.org/https://doi.org/10.1016/j.progpolymsci.2013.06.003.

(12) Nezakati, T.; Seifalian, A.; Tan, A.; Seifalian, A. M. Conductive Polymers: Opportunities and Challenges in Biomedical Applications. *Chem. Rev.* **2018**, *118* (14), 6766–6843. https://doi.org/10.1021/acs.chemrev.6b00275.

(13) Wan, A. M. D.; Schur, R. M.; Ober, C. K.; Fischbach, C.; Gourdon, D.; Malliaras, G. G. Electrical Control of Protein Conformation. *Adv. Mater.* **2012**, *24* (18), 2501–2505. https://doi.org/10.1002/adma.201200436.

(14) Gkoupidenis, P.; Schaefer, N.; Garlan, B.; Malliaras, G. G. Neuromorphic Functions in PEDOT:PSS Organic Electrochemical Transistors. *Adv. Mater.* **2015**,

27 (44), 7176–7180. https://doi.org/10.1002/adma.201503674.

(15) Inal, S.; Rivnay, J.; Hofmann, A. I.; Uguz, I.; Mumtaz, M.; Katsigiannopoulos, D.; Brochon, C.; Cloutet, E.; Hadziioannou, G.; Malliaras, G. G. Organic Electrochemical Transistors Based on PEDOT with Different Anionic Polyelectrolyte Dopants. *J. Polym. Sci. Part B Polym. Phys.* **2016**, *54* (2), 147–151. https://doi.org/10.1002/polb.23938.

(16) Dubal, D. P.; Ayyad, O.; Ruiz, V.; Gómez-Romero, P. Hybrid Energy Storage: The Merging of Battery and Supercapacitor Chemistries. *Chem. Soc. Rev.* **2015**, *44* (7), 1777–1790. https://doi.org/10.1039/C4CS00266K.

(17) Campana, A.; Cramer, T.; Simon, D. T.; Berggren, M.; Biscarini, F. Electrocardiographic Recording with Conformable Organic Electrochemical Transistor Fabricated on Resorbable Bioscaffold. *Adv. Mater.* **2014**, *26* (23), 3874–3878. https://doi.org/10.1002/adma.201400263.

(18) Wan, A. M.-D.; Inal, S.; Williams, T.; Wang, K.; Leleux, P.; Estevez, L.; Giannelis, E. P.; Fischbach, C.; Malliaras, G. G.; Gourdon, D. 3D Conducting Polymer Platforms for Electrical Control of Protein Conformation and Cellular Functions. *J. Mater. Chem. B* **2015**, *3* (25), 5040–5048. https://doi.org/10.1039/C5TB00390C.

(19) Guex, A. G.; Puetzer, J. L.; Armgarth, A.;

Littmann, E.; Stavrinidou, E.; Giannelis, E. P.; Malliaras, G. G.; Stevens, M. M. Highly Porous Scaffolds of PEDOT:PSS for Bone Tissue Engineering. *Acta Biomater.* **2017**, *62*, 91–101. https://doi.org/10.1016/j.actbio.2017.08.045.

(20) Mantione, D.; del Agua, I.; Schaafsma, W.; Diez-Garcia, J.; Castro, B.; Sardon, H.; Mecerreyes, D. Poly(3,4-Ethylenedioxythiophene):GlycosAminoGlycan Aqueous Dispersions: Toward Electrically Conductive Bioactive Materials for Neural Interfaces. *Macromol. Biosci.* **2016**, *16* (8), 1227–1238. https://doi.org/10.1002/mabi.201600059.

(21) del Agua, I.; Marina, S.; Pitsalidis, C.; Mantione, D.; Ferro, M.; Iandolo, D.; Sanchez-Sanchez, A.; Malliaras, G. G.; Owens, R. M.; Mecerreyes, D. Conducting Polymer Scaffolds Based on Poly(3,4-Ethylenedioxythiophene) and Xanthan Gum for Live-Cell Monitoring. *ACS Omega* **2018**, *3* (7), 7424–7431. https://doi.org/10.1021/acsomega.8b00458.

(22) Choi, J. S.; Park, J. S.; Kim, B.; Lee, B.-T.; Yim, J.-H. In Vitro Biocompatibility of Vapour Phase Polymerised Conductive Scaffolds for Cell Lines. *Polymer (Guildf).* **2017**, *124*, 95–100. https://doi.org/https://doi.org/10.1016/j.polymer.2017.07.047.

(23) Rauti, R.; Musto, M.; Bosi, S.; Prato, M.;

Ballerini, L. Properties and Behavior of Carbon Nanomaterials When Interfacing Neuronal Cells: How Far Have We Come? *Carbon N. Y.* **2019**, *143*, 430–446. https://doi.org/https://doi.org/10.1016/j.carbon.2018.11.026.

(24) De Volder, M. F. L.; Tawfick, S. H.; Baughman, R. H.; Hart, A. J. Carbon Nanotubes: Present and Future Commercial Applications. *Science (80-.).* **2013**, *339* (6119), 535 LP – 539. https://doi.org/10.1126/science.1222453.

(25) Ebbesen, T. W.; Lezec, H. J.; Hiura, H.; Bennett, J. W.; Ghaemi, H. F.; Thio, T. Electrical Conductivity of Individual Carbon Nanotubes. *Nature* **1996**, *382* (6586), 54–56. https://doi.org/10.1038/382054a0.

(26) Lovat, V.; Pantarotto, D.; Lagostena, L.; Cacciari, B.; Grandolfo, M.; Righi, M.; Spalluto, G.; Prato, M.; Ballerini, L. Carbon Nanotube Substrates Boost Neuronal Electrical Signaling. *Nano Lett.* **2005**, *5* (6), 1107–1110. https://doi.org/10.1021/nl050637m.

(27) Mazzatenta, A.; Giugliano, M.; Campidelli, S.; Gambazzi, L.; Businaro, L.; Markram, H.; Prato, M.; Ballerini, L. Interfacing Neurons with Carbon Nanotubes: Electrical Signal Transfer and Synaptic Stimulation in Cultured Brain Circuits. *J. Neurosci.* **2007**, *27* (26), 6931–6936. https://doi.org/10.1523/JNEUROSCI.1051-07.2007.

(28) Martinelli, V.; Cellot, G.; Toma, F. M.; Long, C. S.; Caldwell, J. H.; Zentilin, L.; Giacca, M.; Turco, A.; Prato, M.; Ballerini, L.; et al. Carbon Nanotubes Promote Growth and Spontaneous Electrical Activity in Cultured Cardiac Myocytes. *Nano Lett.* **2012**, *12* (4), 1831–1838. https://doi.org/10.1021/nl204064s.

(29) Peña, B.; Bosi, S.; Aguado, B. A.; Borin, D.; Farnsworth, N. L.; Dobrinskikh, E.; Rowland, T. J.; Martinelli, V.; Jeong, M.; Taylor, M. R. G.; et al. Injectable Carbon Nanotube-Functionalized Reverse Thermal Gel Promotes Cardiomyocytes Survival and Maturation. *ACS Appl. Mater. Interfaces* **2017**, *9* (37), 31645–31656. https://doi.org/10.1021/acsami.7b11438.

(30) Martinelli, V.; Bosi, S.; Peña, B.; Baj, G.; Long, C. S.; Sbaizero, O.; Giacca, M.; Prato, M.; Mestroni, L. 3D Carbon-Nanotube-Based Composites for Cardiac Tissue Engineering. *ACS Appl. Bio Mater.* **2018**, *1* (5), 1530–1537. https://doi.org/10.1021/acsabm.8b00440.

(31) Bosi, S.; Rauti, R.; Laishram, J.; Turco, A.; Lonardoni, D.; Nieus, T.; Prato, M.; Scaini, D.; Ballerini, L. From 2D to 3D: Novel Nanostructured Scaffolds to Investigate Signalling in Reconstructed Neuronal Networks. *Sci. Rep.* **2015**, *5*, 9562.

(32) Aurand, E. R.; Usmani, S.; Medelin, M.; Scaini, D.; Bosi, S.; Rosselli, F. B.; Donato, S.; Tromba, G.; Prato, M.; Ballerini, L. Nanostructures to Engineer 3D

Neural-Interfaces: Directing Axonal Navigation toward Successful Bridging of Spinal Segments. *Adv. Funct. Mater.* **2018**, *28* (12), 1700550. https://doi.org/10.1002/adfm.201700550.

(33) Bosi, S.; Fabbro, A.; Cantarutti, C.; Mihajlovic, M.; Ballerini, L.; Prato, M. Carbon Based Substrates for Interfacing Neurons: Comparing Pristine with Functionalized Carbon Nanotubes Effects on Cultured Neuronal Networks. *Carbon N. Y.* **2016**, *97*, 87–91. https://doi.org/https://doi.org/10.1016/j.carbon.2015.07.074.

(34) Alegret, N.; Dominguez-Alfaro, A.; González-Domínguez, J. M.; Arnaiz, B.; Cossío, U.; Bosi, S.; Vázquez, E.; Ramos-Cabrer, P.; Mecerreyes, D.; Prato, M. Three-Dimensional Conductive Scaffolds as Neural Prostheses Based on Carbon Nanotubes and Polypyrrole. *ACS Appl. Mater. Interfaces* **2018**, *10* (50), 43904–43914. https://doi.org/10.1021/acsami.8b16462.

(35) Ali-Boucetta H., Al-Jamal K.T., K. K. Cytotoxic Assessment of Carbon Nanotube Interaction with Cell Cultures. *Methods Mol. Biol. (Methods Protoc.* **2011**, *726*.

(36) Winther-Jensen, B.; Chen, J.; West, K.; Wallace, G. Vapor Phase Polymerization of Pyrrole and Thiophene Using Iron(III) Sulfonates as Oxidizing Agents. *Macromolecules* **2004**, *37* (16), 5930–5935. https://doi.org/10.1021/ma049365k.

(37) Winther-Jensen, B.; West, K. Vapor-Phase Polymerization of 3,4-Ethylenedioxythiophene: A Route to Highly Conducting Polymer Surface Layers. *Macromolecules* **2004**, *37* (12), 4538–4543. https://doi.org/10.1021/ma049864l.

(38) Brooke, R.; Cottis, P.; Talemi, P.; Fabretto, M.; Murphy, P.; Evans, D. Recent Advances in the Synthesis of Conducting Polymers from the Vapour Phase. *Prog. Mater. Sci.* **2017**, *86*, 127–146. https://doi.org/https://doi.org/10.1016/j.pmatsci.2017.01.004.

(39) Wu, D.; Zhang, J.; Dong, W.; Chen, H.; Huang, X.; Sun, B.; Chen, L. Temperature Dependent Conductivity of Vapor-Phase Polymerized PEDOT Films. *Synth. Met.* **2013**, *176*, 86–91. https://doi.org/https://doi.org/10.1016/j.synthmet.2013.05.033.

(40) Fabretto, M.; Zuber, K.; Hall, C.; Murphy, P.; Griesser, H. J. The Role of Water in the Synthesis and Performance of Vapour Phase Polymerised PEDOT Electrochromic Devices. *J. Mater. Chem.* **2009**, *19* (42), 7871–7878. https://doi.org/10.1039/B912324E.

(41) Mueller, M.; Fabretto, M.; Evans, D.; Hojati-Talemi, P.; Gruber, C.; Murphy, P. Vacuum Vapour Phase Polymerization of High Conductivity PEDOT: Role of PEG-PPG-PEG, the Origin of Water, and Choice of Oxidant.

Polymer (Guildf). **2012,** *53* (11), 2146–2151. https://doi.org/https://doi.org/10.1016/j.polymer.2012.03.028.

(42) Karimi, A.; Shojaei, A.; Tehrani, P. Mechanical Properties of the Human Spinal Cord under the Compressive Loading. *J. Chem. Neuroanat.* **2017**, *86*, 15–18. https://doi.org/https://doi.org/10.1016/j.jchemneu.2017.07.004.

(43) Budday, S.; Nay, R.; de Rooij, R.; Steinmann, P.; Wyrobek, T.; Ovaert, T. C.; Kuhl, E. Mechanical Properties of Gray and White Matter Brain Tissue by Indentation. *J. Mech. Behav. Biomed. Mater.* **2015**, *46*, 318–330. https://doi.org/10.1016/j.jmbbm.2015.02.024.

(44) Choi, J. W.; Han, M. G.; Kim, S. Y.; Oh, S. G.; Im, S. S. Poly(3,4-Ethylenedioxythiophene) Nanoparticles Prepared in Aqueous DBSA Solutions. *Synth. Met.* **2004,** *141* (3), 293–299. https://doi.org/https://doi.org/10.1016/S0379-6779(03)00419-3.

(45) Mao, H.; Liu, X.; Chao, D.; Cui, L.; Li, Y.; Zhang, W.; Wang, C. Preparation of Unique PEDOT Nanorods with a Couple of Cuspate Tips by Reverse Interfacial Polymerization and Their Electrocatalytic Application to Detect Nitrite. *J. Mater. Chem.* **2010,** *20* (45), 10277–10284. https://doi.org/10.1039/C0JM01745K.

(46) Bai, X.; Hu, X.; Zhou, S.; Yan, J.; Sun, C.; Chen, P.; Li, L. Controlled Fabrication of Highly Conductive Three-Dimensional Flowerlike Poly (3{,}4-Ethylenedioxythiophene) Nanostructures. *J. Mater. Chem.* **2011**, *21* (20), 7123–7129. https://doi.org/10.1039/C1JM10335K.

(47) Zengin, H.; Zhou, W.; Jin, J.; Czerw, R.; Smith Jr., D. W.; Echegoyen, L.; Carroll, D. L.; Foulger, S. H.; Ballato, J. Carbon Nanotube Doped Polyaniline. *Adv. Mater.* **2002**, *14* (20), 1480–1483. https://doi.org/10.1002/1521-4095(20021016)14:20<1480::AID-ADMA1480>3.0.CO;2-O.

(48) Arcila-Velez, M. R.; Emmett, R. K.; Karakaya, M.; Podila, R.; Díaz-Orellana, K. P.; Rao, A. M.; Roberts, M. E. A Facile and Scalable Approach to Fabricating Free-Standing Polymer—Carbon Nanotube Composite Electrodes. *Synth. Met.* **2016**, *215*, 35–40. https://doi.org/https://doi.org/10.1016/j.synthmet.2016.02.005.

(49) Hu, X.; Chen, G.; Wang, X. An Unusual Coral-like Morphology for Composites of Poly(3,4-Ethylenedioxythiophene)/Carbon Nanotube and the Enhanced Thermoelectric Performance. *Compos. Sci. Technol.* **2017**, *144*, 43–50. https://doi.org/https://doi.org/10.1016/j.compscitech.2017.03.018.

(50) Dyke, C. A.; Tour, J. M., Overcoming the Insolubility of Carbon Nanotubes Through High Degrees of Sidewall Functionalization. *Chem. Eur. J.* **2004**, *10* (4), 812-817. https://doi.org/10.1002/chem.200305534

(51) Wei, B.; Liu, J.; Ouyang, L.; Martin, D. C. POSS-ProDOT Crosslinking of PEDOT. *J. Mater. Chem. B* **2017**, *5* (25), 5019–5026. https://doi.org/10.1039/C7TB00598A.

(52) Wang, S.; Sun, C.; Guan, S.; Li, W.; Xu, J.; Ge, D.; Zhuang, M.; Liu, T.; Ma, X. Chitosan/Gelatin Porous Scaffolds Assembled with Conductive Poly(3{,}4-Ethylenedioxythiophene) Nanoparticles for Neural Tissue Engineering. *J. Mater. Chem. B* **2017**, *5* (24), 4774–4788. https://doi.org/10.1039/C7TB00608J.

(53) Wang, S.; Guan, S.; Zhu, Z.; Li, W.; Liu, T.; Ma, X. Hyaluronic Acid Doped-Poly(3,4-Ethylenedioxythiophene)/Chitosan/Gelatin (PEDOT-HA/Cs/Gel) Porous Conductive Scaffold for Nerve Regeneration. *Mater. Sci. Eng. C* **2017**, *71*, 308–316. https://doi.org/https://doi.org/10.1016/j.msec.2016.10.029.

(54) Wang, S.; Guan, S.; Xu, J.; Li, W.; Ge, D.; Sun, C.; Liu, T.; Ma, X. Neural Stem Cell Proliferation and Differentiation in the Conductive PEDOT-HA/Cs/Gel Scaffold for Neural Tissue Engineering. *Biomater. Sci.* **2017**, *5* (10), 2024–2034. https://doi.org/10.1039/C7BM00633K.

(55) Porada, S.; Zhao, R.; van der Wal, A.; Presser, V.; Biesheuvel, P. M. Review on the Science and Technology of Water Desalination by Capacitive Deionization. *Prog. Mater. Sci.* **2013**, *58* (8), 1388–1442. https://doi.org/https://doi.org/10.1016/j.pmatsci.2013.03.005.

(56) Katiyar, K. S.; Winter, C. C.; Struzyna, L. A.; Harris, J. P.; Cullen, D. K. Mechanical Elongation of Astrocyte Processes to Create Living Scaffolds for Nervous System Regeneration. *J. Tissue Eng. Regen. Med.* **2017**, *11* (10), 2737–2751. https://doi.org/10.1002/term.2168.